Mechatronics 23 (2013) 94–107

Contents lists available at SciVerse ScienceDirect

Mechatronics

journal homepage: www.elsevier.com/locate/mechatronics

A control and automation system for wave basins

P.C. de Mello, M.L. Carneiro, E.A. Tannuri *, F. Kassab Jr., R.P. Marques, J.C. Adamowski, K. Nishimoto

Escola Politécnica, University of São Paulo, Brazil

ARTICLE INFO

Article history:
Received 27 December 2011
Accepted 22 November 2012
Available online 27 December 2012

Keywords:
Wave tank
Wave generation
Automation
Wave probe
Wavemaker
Realtime system
PLC

ABSTRACT

This paper presents the new active absorption wave basin, named Hydrodynamic Calibrator (HC), constructed at the University of São Paulo (USP), in the Laboratory facilities of the Numerical Offshore Tank (TPN). The square (14 m × 14 m) tank is able to generate and absorb waves from 0.5 Hz to 2.0 Hz, by means of 148 active hinged flap wave makers. An independent mechanical system drives each flap by means of a 1HP servo-motor and a ball-screw based transmission system. A customized ultrasonic wave probe is installed in each flap, and is responsible for measuring wave elevation in the flap. A complex automation architecture was implemented, with three Programmable Logic Computers (PLCs), and a low-level software is responsible for all the interlocks and maintenance functions of the tank. Furthermore, all the control algorithms for the generation and absorption are implemented using higher level software (MATLAB®/Simulink block diagrams). These algorithms calculate the motions of the wave makers both to generate and absorb the required wave field by taking into account the layout of the flaps and the limits of wave generation. The experimental transfer function that relates the flap amplitude to the wave elevation amplitude is used for the calculation of the motion of each flap. This paper describes the main features of the tank, followed by a detailed presentation of the whole automation system. It includes the measuring devices, signal conditioning, PLC and network architecture, real-time and synchronizing software and motor control loop. Finally, a validation of the whole automation system is presented, by means of the experimental analysis of the transfer function of the waves generated and the calculation of all the delays introduced by the automation system.

1. Introduction

The dynamic response of offshore structures, vessels and equipment can be studied by means of reduced scale experiments in oceanic wave basins. They can reproduce the environmental conditions of offshore conditions, using wave, current and wind generators.

Wave generators have been developed in the last six decades, aiming to reproduce the complex wave pattern encountered in real sea, including multi-directionality, as presented by Biesel [1]. He proposed the utilization of a segmented generator, composed of a large number of independent actuators. This type of generator is able to reproduce the multi-directionality of real sea state, by changing the phase of the motion of each actuator, in a "snake" like movement. As the tanks present limited dimensions, the waves reflected on the opposite side interfere with the incident wave-pattern on the structure or vessel being tested. A passive apparatus is used for absorbing the waves on the opposite side of the Basin. "Beach"-like structures or a set of small particles in a grid are solutions normally deployed [3]. However, passive systems are tuned for wave-absorption only in a reduced range of frequencies [5].

Another way to solve the interference of the reflected waves is to use very large basins. For some kinds of experiments, typically in regular and transient waves, in large basins there is sufficient time to evaluate the response of offshore structures before the unwanted reflections corrupt the signals. The time windows available for tests can be determined by the distances between model and tank borders and the wave celerity. In addition, the waves reflected or diffracted by the model decrease with the distance of the model, and they may be small when reaching the tank borders.

In order to obtain a better performance for a broader range of frequencies, new generators with the ability of both generating waves and absorbing the reflected waves have been studied in the last two decades. These wave basins use wave feedback measuring device and a closed loop control system to absorb waves, such as the systems presented by Schäffer and Klopman [16], Maeda et al. [7] and Naito [11,12]. Furthermore, small dimension tanks may be used with active wave absorption, performing long duration tests normally applied in irregular wave analysis.

The most innovative type of wave tanks are those counting on independent generation/absorption actuators all along the whole perimeter. The tank is then able to generate multi-directional

* Corresponding author. Address: Departamento de Engenharia Mecatrônica e Sistemas Mecânicos, Tanque de Provas Numérico TPN-USP, Av. Prof. Mello Moraes, 2231 – Cidade Universitária, São Paulo, SP CEP 05508-030, Brazil. Tel.: +55 11 3091 5414.

E-mail address: eduat@usp.br (E.A. Tannuri).

0957-4158/$ - see front matter © 2012 Elsevier Ltd. All rights reserved.
http://dx.doi.org/10.1016/j.mechatronics.2012.11.004

waves and to absorb all the components that reach the other side of the tank. Extra features such as bimodal waves and time-changing wave direction can also be reproduced in these tanks. Furthermore, the total dimension of the tank can be reduced, since the active absorption algorithm can be tuned or adjusted for the required frequency range. It allows the execution of a variety of hydrodynamic experiments. When a model under test is very reflective, the actuators absorb this reflected wave to prevent unwanted re-reflections that would distort the incident wave field. The time-changing wave direction is a desirable feature that is also possible to reproduce with this type of wave basin. This phenomenon is usual in the Brazilian offshore oil fields. Another advantage of this type of tank is the possibility to change the wave relative heading by changing the wave direction, and not the heading of the moored model itself. Without this feature, each relative angle requires a new mooring and set-up arrangement, which is much more time-consuming than a simple change in the wave direction.

This work presents the development of a new hydrodynamic test basin (HC), developed at USP (University of São Paulo). The wave basin is composed of 148 independent actuators distributed along its 14 m × 14 m square perimeter. Each of them is driven by a servo-motor and a ball screw mechanism, and has an ultrasonic wave-sensor for feedback to the absorption control system.

The HC adopted a solution fully based on PLC (programmable logic controller). This solution required an adequate specification of the equipment and network interfaces, and a detailed analysis of their time-charts. This solution keeps the advantages of industrial automation (robustness, reliability, maintenance) while still satisfying the performance and IO requirements of the wave tank application.

This paper describes the main features of the HC, followed by a detailed presentation of the whole automation system. It includes the measuring devices, signal conditioning, PLC and network architecture, real-time and synchronizing software and motor control loop. Finally, a validation of the whole automation system is presented, by means of the experimental analysis of the transfer function of the generated waves and the calculation of all the delays introduced by the automation system. To achieve these features of operability, the response of all the equipment was taken into account in the analyses of the system. The actuator had to be as fast as possible to minimize the time lag with a minimum attenuation. The response of the wave-sensors needs to be accurately known, in order to design compensations at the control systems. The design of the proper wave active absorption algorithm is based on synthesizing a digital filter with the compensation of the actuator and sensor dynamics, wave response and automation delays.

2. Description of the wave basin

The HC is a 14 m × 14 m square tank, with 4.1 m water depth. There are 39 hinged flaps on each side of the tank. In order to avoid collision, two actuators are blocked in each edge of the tank. The immersed length of the flap is 1.21 m, considering the distance from the joint to the water line. Fig. 2.1 shows a photo of the tank when generating a regular wave of 0.7 Hz with a model under test. Fig. 2.2 shows the tank plan, including the reference system and the flap numbering.

Finally, Fig. 2.3 shows the driving mechanism of the hinged flap. Brushless 750 W motors and a ball-screw linear actuator are used in each of them. A frame-type structure supports five mechanisms, and it is attached to the reinforced concrete by means of screws and bolts, providing acceptable reaction forces for both vertical and horizontal motions, as shown in Fig. 2.4.

Since a spurious wave pattern can be generated behind the flaps, a passive absorption system was installed, comprising a beach and an absorption mesh (see in Fig. 2.5).

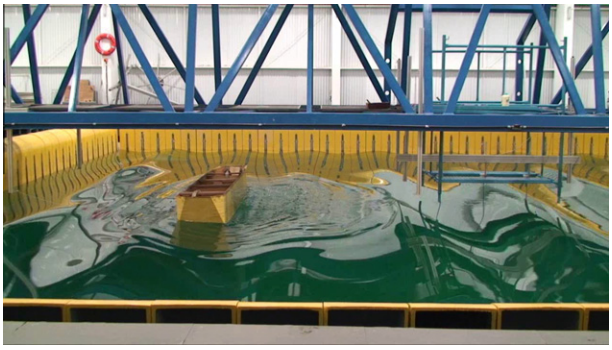

Fig. 2.1. Wave tank of the HC-TPN.

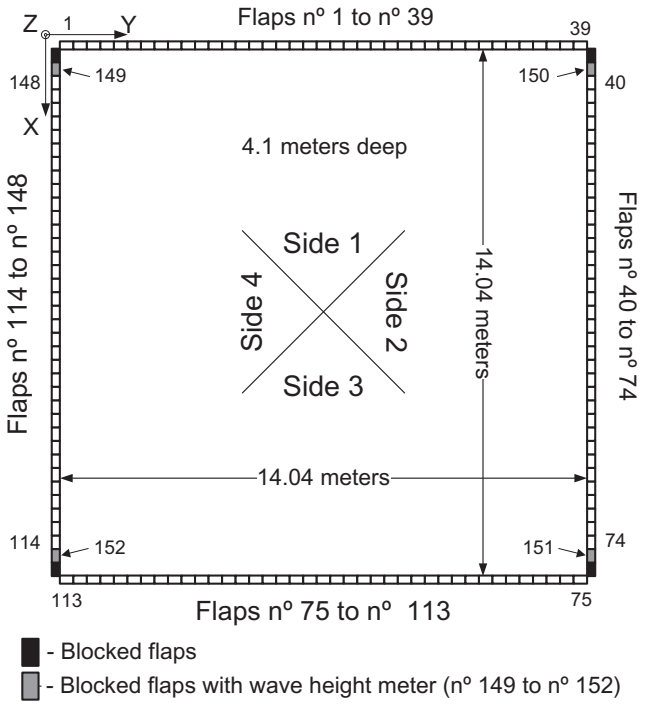

Fig. 2.2. Numbering reference system of the wave generator.

The signal-conditioning boards of the wave-probes are installed right behind the mechanism. This position is very close to the flaps, and prevents electromagnetic noise from corrupting the electric signal of the ultrasonic transducers. The transmission to the PLCs is then done by 4–20 mA current signal, not affected by noise.

3. System automation

3.1. Ultrasonic wave probes

The ultrasonic wave probes are based on the pulse-echo technique. The distance between the submerged transducer and the water surface is calculated as the product of the time of flight of the ultrasonic pulse between transducer and the waterline and the sound speed in water. The sound speed in water is corrected according to the measured water temperature.

The broadband piezoelectric ultrasonic transducer has a 2 MHz-center frequency. It is installed on the wave board, at a distance of 385 mm from the calm water surface. A wave-guide is installed on the surface of each in order to guarantee that a sufficient amount of wave-energy returns to the transducer after the reflection.

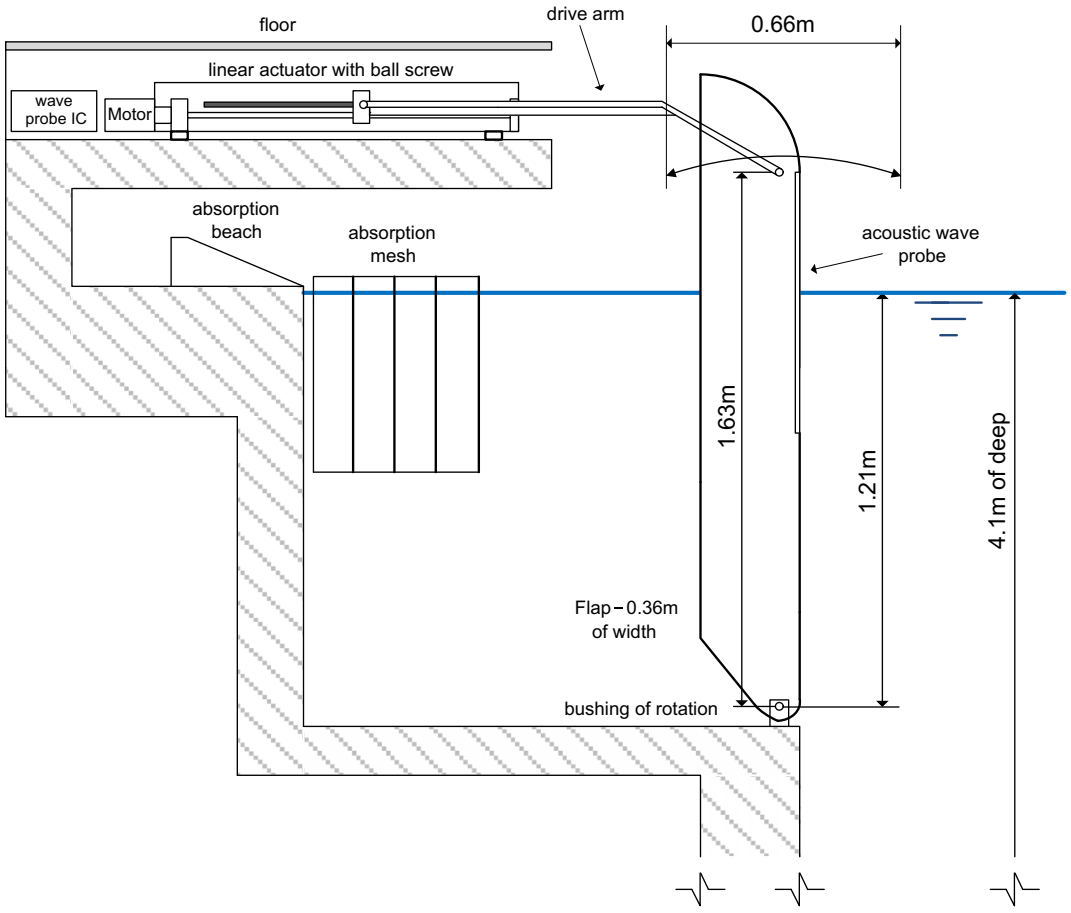

Fig. 2.3. Hinged flap driving mechanism.

Fig. 2.4. Linear actuators of the wave generators.

Furthermore, it avoids signal losses when the ultrasonic pulse reflects on the inclined water surface. The wave guide has two rows of holes that guarantee the same water level inside and outside the guide. The successive reflections along the wave guide (Fig. 3.1a) may cause some spreading in the echo signal, but only the first arrival is measured. The wave guide can be seen in Fig. 3.1c and the assembly on the hinged flap is shown in Fig. 3.1d. The shape of the reflected pulse is shown in Fig. 3.1b for different moments along a wave. Some modification in the pulse shape can be verified due to the inclination of the surface. The pulse detection algorithm can deal with it [8].

An electronic board was designed for signal conditioning and transmission. Each board can control six wave probes, and 32 boards were used in the tank. Each wave probe channel has independent circuitry for pulse generation, signal amplification and echo detection. The returning time is measured by a PIC

Fig. 2.5. Absorption mesh in the space behind the flaps.

18F1220-I/P micro-controller, and the scan time is 9.6 ms (104.1 Hz). An external signal from the automation system enables each board. Furthermore, a 4–20 mA analog output is provided for each channel, using 16-bit Analog Devices AD421 DAC converters. They are connected to the IO input cards of the PLC 3 (see next section). The total delay time of the measurement system is 17.9 ms (9.6 ms scan time added to 8.3 ms DA conversion time).

The pulse generator excites the transducer with 240Vdc short negative pulse, using a MOSFET driver. A 38 dB signal amplifier is used to amplify the echo signal. The accurate definition of the echo is performed by a window-detector (2 semi-cycles) with variable trigger level. If the first positive semi-cycle of the echo is not detected, the second negative semi-cycle may be detected. Hence, the detector measures the echoes of each half wavelength, corresponding to intervals of 0.37 mm (2 MHz acoustic waves in water), increasing the robustness of the sensor in comparison of a simple positive detector. The trigger level is exponentially reduced along time, increasing the robustness of the detection and avoiding false-positive detections. The exponential function was calibrated

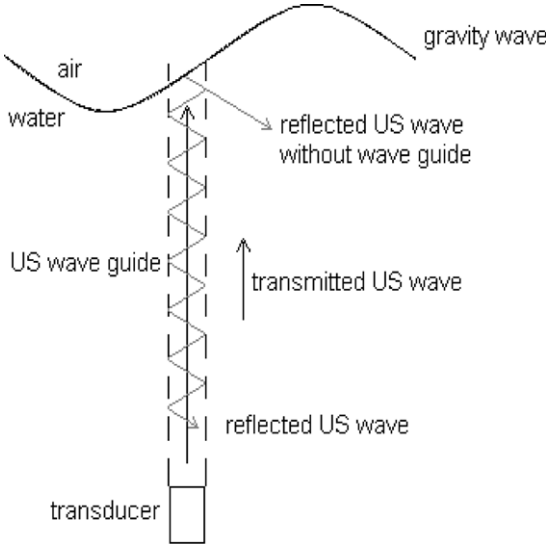

(a)

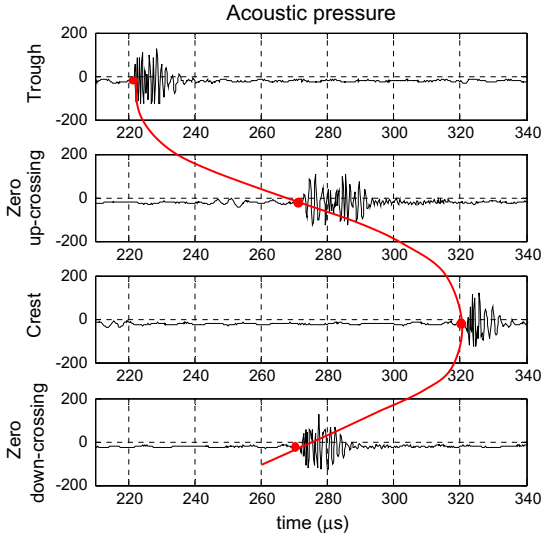

(b)

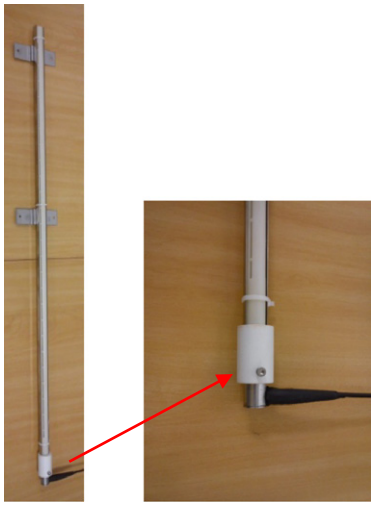

(c)

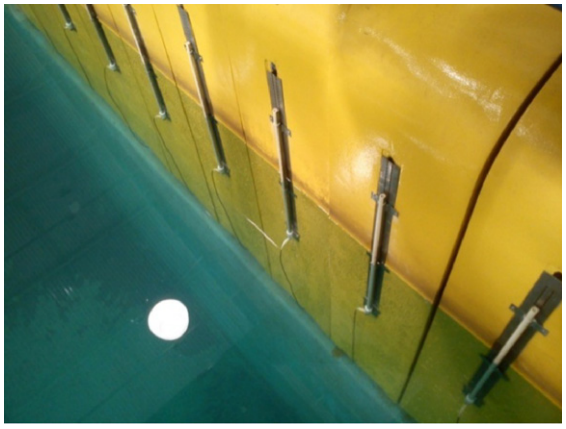

(d)

Fig. 3.1. Ultrasonic wave height meter.

by static tests of the wave guide at several inclinations and water levels. The main sources of false-detection are related to reflection in particles in water, air bubbles inside the guide or wall irregularities along the guide. The variable trigger level is equivalent to a time-varying amplification gain. Fig. 3.2 illustrates the operating principle of the analog circuitry used.

The clock used to measure the echo time of flight is generated by an interruption of a 16-bit timer of the PIC micro-controller. The time resolution is 100 ns, which is equivalent to 0.074 mm. The echo time of flight is evaluated at each sample, and if it is a valid value, it is sent to the DAC. Since the guide length is 775 mm, the maximum returning time is 1.05 ms (10458 counts). The minimum time is defined as 46 μs (equivalent to 33.7 mm), and was calculated in order to avoid the near-field acoustic reflections. Thus, a returning time is considered valid if it lies between 46 μs and 1.05 ms. If a non-valid time is verified, the previous value is sent to the DA converter. After 25 uninterrupted invalid values, a fail mode is activated and the analog output is set to 3.5 mA.

3.2. Control and automation

The PLCs (programmable logic controller) are widely applied for industry and manufactory automation applications. They are equipped with IO cards for a large number of two-state sensors (on–off), some analog sensors and actuators, such as servo-drivers and step-motors. Communication is based on standard protocol at industrial equipments. Robustness, reliability and ease of maintenance are the main pre-requirements for those systems.

Due to the industry needs for higher production velocity, flexibility of maintenance, integration between production and managing, the new industry-based automation and network types of equipment present substantial advances in performance and speed characteristics. This recent evolution allowed the HC to be based on those systems. This solution keeps the advantages of industrial automation while still meeting the performance and IO requirements of the wave tank application.

The HC presents 148 servo-actuators and 152 analog level sensors, and requires a small scan and processing time for guaranteeing the performance of wave-absorption control loop. Hence, besides the PLCs and servo-drivers, a quad-core personal computer (PC) is used for algorithm calculation and an industrial gigabit network for data transfer with PLC.

3.2.1. System topology

The automation system is composed of servo-drivers, motor control CPUs, PLCs and a PC. The whole system is based on Mitsubishi-FA equipment.

Two token-ring optical networks are used for data transfer. The first is a SSCNET network with 1.77 ms scan time, and connects the servo-drivers to the motor-control CPUs. The second is a MELSEC NET-G network (1 Gbps with 1.35 ms scan time), and connects the PLCs to the PC.

The PLCs (Q04UDHCPU) were chosen due to the small time required for processing ladder steps. Basic operations are processed in 9.5 ns, floating point operations in 57 ns and copying instructions in 19 ns. They allow up to 40 k ladder steps and present a high speed data-exchange between the CPU and the bus.

The motor control CPUs (Q173HCPU) are programmed in SFC (structured flow chart) language. They allow up to 64 KB programming codes or 4096 steps, and 63 different instructions are available. The scan time is up to 3.50 ms (including the 1.77 ms of the SSCNET scan time) and there is an additional 1.22 ms of scan time between CPU and PLC.

Fig. 3.3 shows the diagram of the system. PLC 1 has three motor control CPUs and commands 96 hinged flaps, since each CPU sends the instructions to 32 servo-drivers. The PLC 2 has two motor control CPUs and commands the remaining 52 hinged flaps. PLC 3 has 19 IO modules with eight analog-current input each. They are connected to the signal conditioning boards of the ultrasonic wave probes.

The memory allocation map is unique for the NET-G network and PLCs. Each component has write-access to a specific range of addresses, but all of them can read the whole memory. The communication based on shared-memory is an efficient and fast way to integrate the different equipment.

Each module has its own scan time that was considered in the integration of the equipment. The total delay time for the control loop is thus the result of the summation of the scan-time of each equipment.

PLC 1 and 2 have a small scan time (1.20 ms), due to the simplicity of the tasks performed. Their programs only replicate the data from the motor-control CPUs and the NET-G network memory map. The motor control CPUs scan time is 1 ms and the communication between the CPU and PLC is 1.22 ms, and they communicate with the servo-drivers by means of the SSCNET, that presents a scan time of 1.77 ms. PLC 3 executes more demanding tasks, which

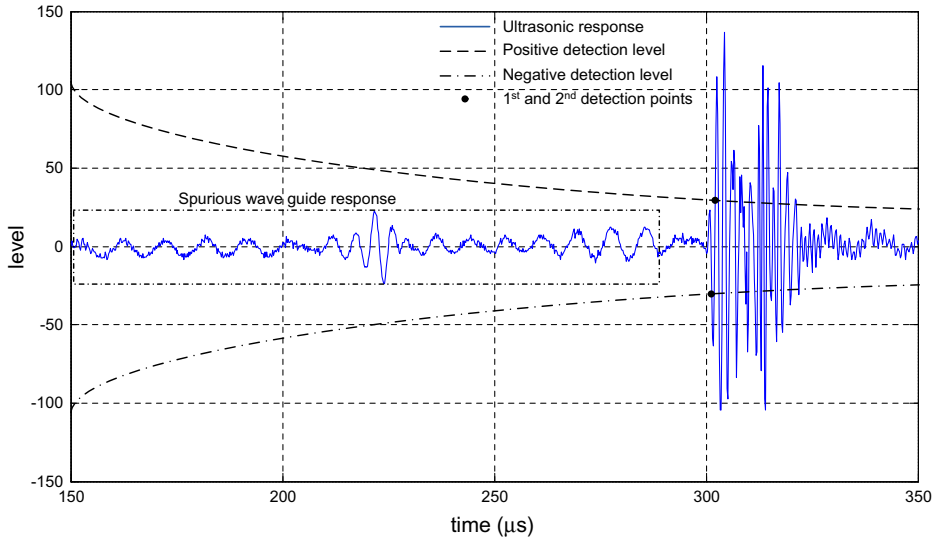

Fig. 3.2. Echo detection response.

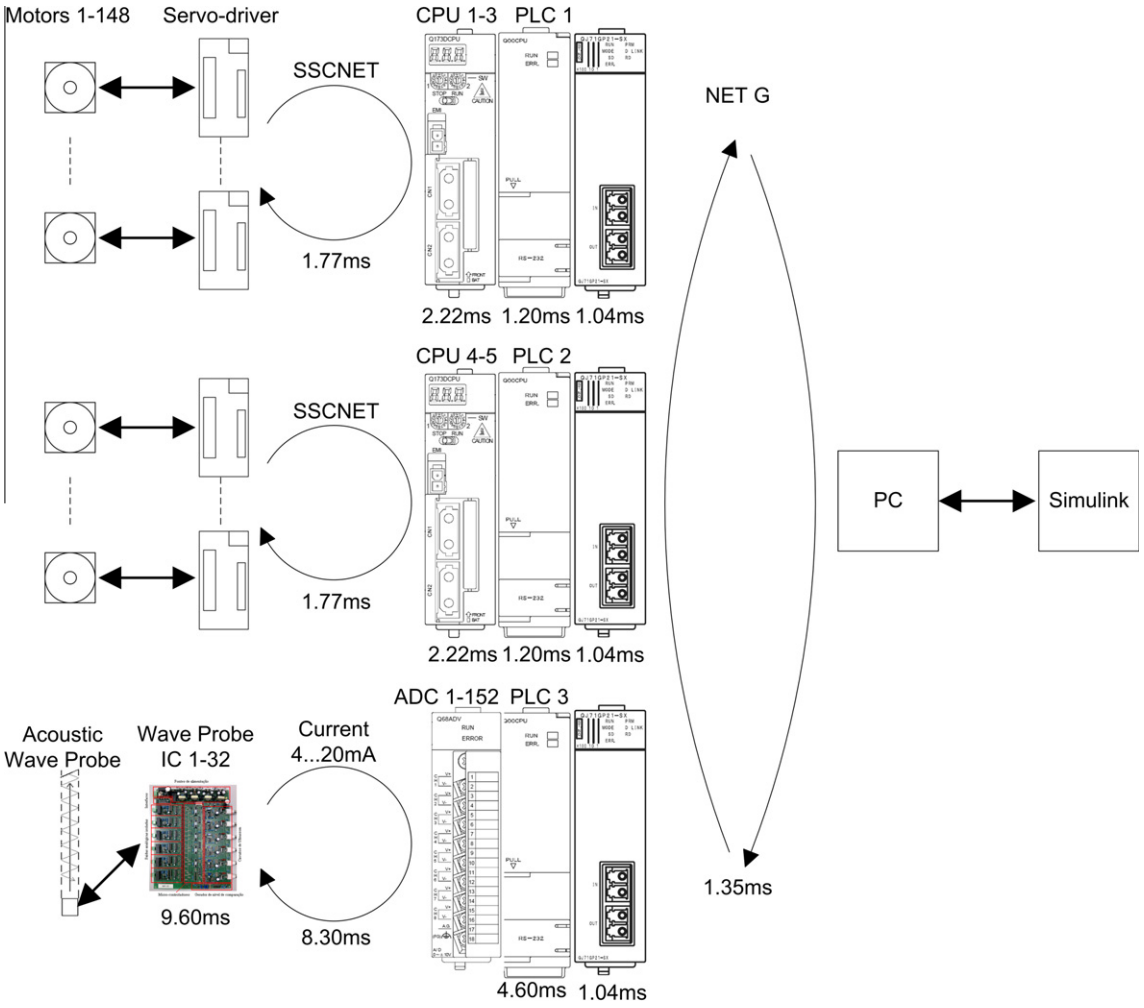

Fig. 3.3. HC-TPN automation system.

justifies the larger scan time (4.60 ms).This PLC performs the reading of the wave-probes measurements and the subtraction of the average level for each sensor.

3.2.2. Real-time state machine

The synchronous data are exchanged between the three PLCs and the PC by a state machine based on the gigabit network communication. The time base is given by a 32-bit counter implemented in PLC 1 (CBT), with a refresh-rate of 12 ms (83.8 Hz). At each sample, new hinged flap positions and velocities are read from the PC and sent to the motor control CPUs. The actual position of the motors (encoders) and the measurements from wave probes are sent to the PC.

The network state machine is implemented by a ladder program in the PLCs and by a C++ program in the PC. The PC commands a network flag-bit (B0) used for initiating the operation. The PC then writes the new flap positions and velocities in the network and increments a 32-bit counter (CPC). The PLCs read the two indicators (B0 and CPC) and start refreshing the data when their internal counter (CPLCx) differs from the CPC counter. PLC 1 and PLC 2 activate the motor control CPUs, read the new positions and velocities from the network and write the encoder real position in the network. PLC 3 activates the wave probe signal conditioners and writes the new values in the network. After that, the PLCs increment their own network counters (CPLCx). The PC reads those counters (CPLCx) and compares them with its own counter (CPC). If all PLC counters are updated (which means that all PLCs have finished their data update), and the time base counter (CBT) is updated, the PC reads all the new data (encoders and wave probes) from the network and sends it to the user interface and control software. After the processing time, new hinged flap positions and velocities are available, the process is re-initiated. When the flag-bit is switched off, the process is finished and all the equipment is set to a stand-by mode. Fig. 3.4 presents the system state diagram.

The user-interface and control was implemented using Matlab/Simulink, due to the complexity of the control algorithms of wave absorption and generation. The hardware interface and PC state machine were implemented in a C++ S-function integrated with the Simulink block diagram, using the Mitsubishi API library for WinXP. This function presents two inputs (vectors of the new calculated flaps position and velocity) and three outputs (vectors of encoder and wave probe measurements and time base counter). The counter was used for experimental definition of the minimum scan time that still guarantees real-time synchronization, and 12.00 ms was the value obtained.

This value is coherent with the delay times shown in Fig. 3.3. The summation of the propagation time from the PC to the PLC 3, and then returning to the PC results 9.38 ms:

$$t_S = 1.35\ \text{ms} + 1.04\ \text{ms} + 4.60\ \text{ms} + 1.04\ \text{ms} + 1.35\ \text{ms} = 9.38\ \text{ms} \quad (1)$$

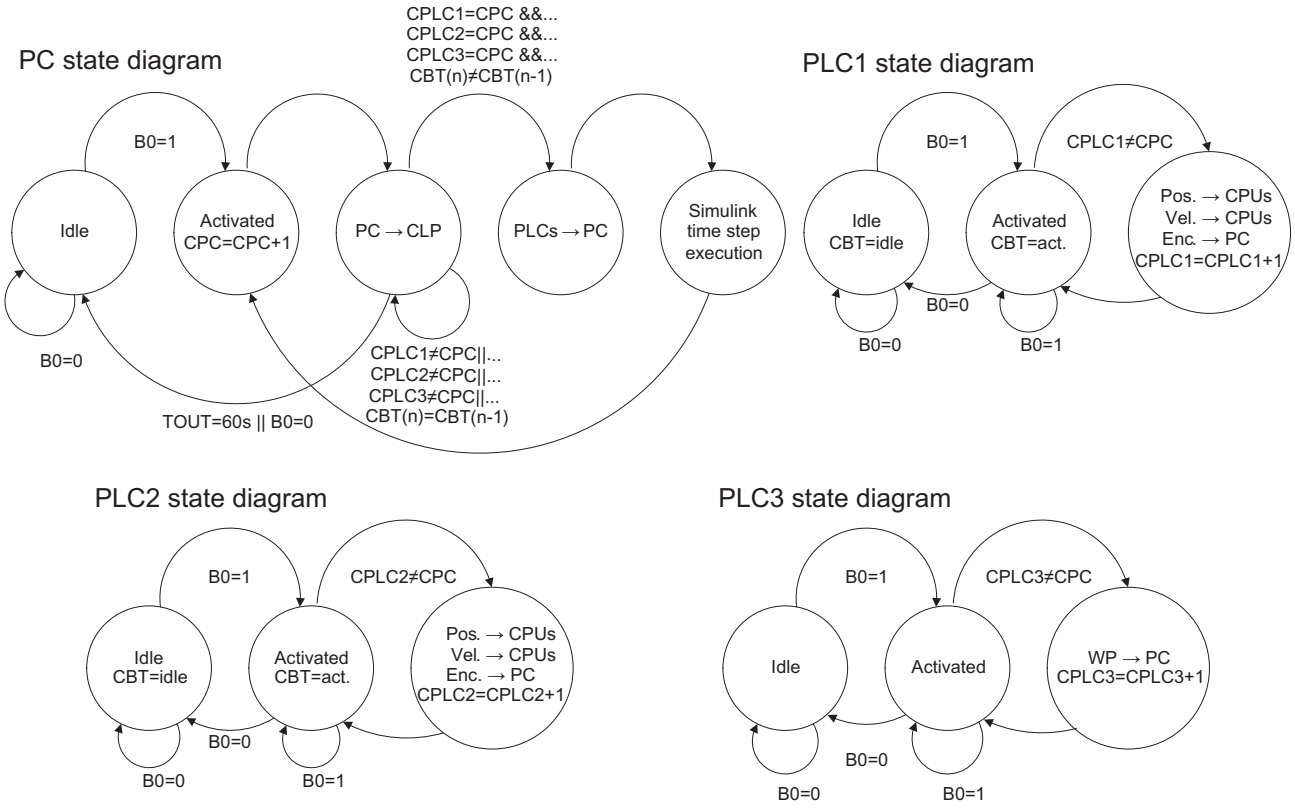

Fig. 3.4. Real-time state machine.

The processing time of the control algorithm implemented in Simulink is approximately 2 ms, and the scan time can be changed in steps of 2.00 ms (due to the resolution of the counter). Hence, the value of 12.00 ms is clearly justified.

3.3. Motor control

Motor control CPU contains the general automation tasks related to the hinged flap motion devices. Tasks such as the initialization of each one of the 32 servo-drives, micro-switch referencing, return to the zero position and wave generation are all activated by selector bits controlled by the PLCs. Thus, the interlocking between servo-driver and CPU occurs through complex tasks that, from the point of view of the PLC, are simplified by a set of operational modes.

The motion control loop is implemented inside the servo-driver in a 1.1 ms sample rate. The position and velocity references are sent to the servo-driver at each 12 ms scan time, and the feedback signal comes from the encoder. Fig. 3.5 shows the motion control loop. It is composed of three PID cascaded loops. The first one is the torque control, which uses the current as the feedback signal. It receives the reference from the velocity control loop, the feedback signal of which is obtained by the numerical derivative of the encoder measurement. The flap velocity reference is used as the maximum limiting velocity. Finally, the position loop also presents a feedforward term (not indicated in the figure) that applies part of the position error directly to the velocity loop, in order to reduce the tracking error. An auto-tuning algorithm is activated for online adjustment of the gains (position and velocity loops). According to Mitsubishi [10], the auto-tuning uses a reference response table related to the machine stiffness. Only two parameters are necessary to set the auto-tuning; machine stiffness (in the present case, this parameter was adjusted to 85.2 Hz resonance frequency), and the ratio between the load inertia and machine inertia (in the present case, this value was adjusted to 5).

The dynamic model of the closed loop servo-motor is necessary for the wave generation and absorption algorithms. Hence, several tests were performed in order to identify the system, using ramp, impulse and chirp signals. The result is a second order dynamic system (corresponding to the mechanical system and control loop) in series with a delay of 12 ms (corresponding to one sample time). The dynamic term frequency response is presented in Fig. 3.6, comparing it to a standard second-order system with 106.48 rad/s natural frequency and 0.95 damping factor. The same conclusion

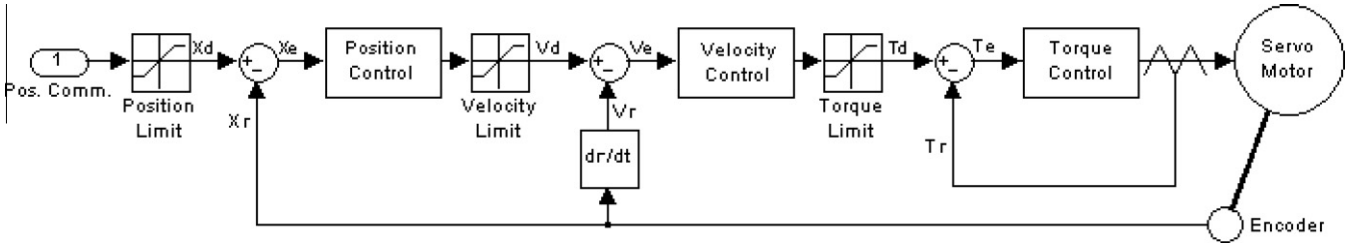

Fig. 3.5. Position control loop running inside the servo-motor.

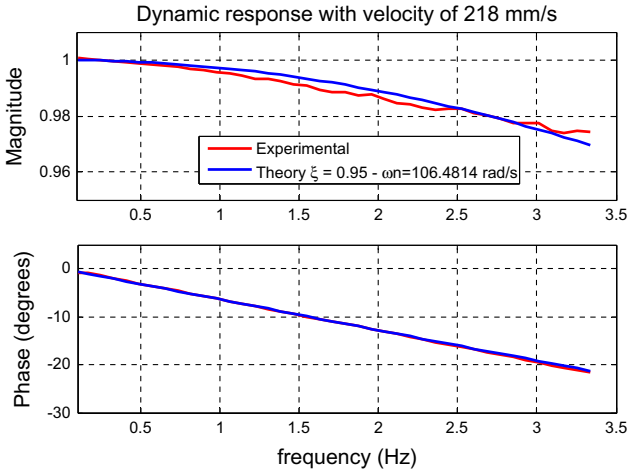

Fig. 3.6. System dynamic response.

could be drawn considering any reference signal (ramp, impulse or chirp).

4. Wave generation response

4.1. Wave generation transfer function

The wave generation transfer function is the relation between the amplitude motion at the still water level of the hinged flap and the amplitude of the generated wave in any defined point of the tank. The comparison between the theoretical and experimental transfer function may be considered a complete experiment for the validation of the response of the whole automation system, wave probes and motion control.

The theoretical transfer function has two hydrodynamic terms. The first one is the progressive wave, which is related to the generated wave away from the wave board. The second is the summation of the evanescent waves, which present an exponential decay with the distance from the wave board. Normally, those waves are not significant after a distance of three wave lengths from the generator. This term comes from the difference between the orbital wave motion and the boundary motion defined by the hinged flap. In the present comparison, the wave measurements come from the wave probes installed on the flaps, and the evanescent modes must be considered according to the linear wave maker theory exposed by Dean and Dalrymple [6] and Zhang [18], summarized below.

For the hinged flap type wave maker used in the HC, it is possible to describe the transfer function in the flap (FT) as a summation of progressive (FT_p) and evanescent (FT_e) waves as:

$$FT = \frac{H_e}{S} + i \cdot \frac{H}{S} = FT_e + i \cdot FT_p \tag{2}$$

here, H_e is the evanescent wave height, H is the progressive wave height, S is the actuator stroke (peak-to-peak excursion) at still water level and i is the unit imaginary number. There is a 90° phase shift between the terms; the total transfer function (FT) thus has a different phase for each wave frequency. The progressive transfer function is given by:

$$FT_p = c_0 \frac{k}{k_x} = c_0 \frac{1}{cos\theta} \tag{3}$$

$$c_0 = \frac{4\sinh kh[\cosh k(-l) - \cosh kh - k(-2l)\sinh k(-l) + k(h+l)\sinh kh]}{k(h+l)(2kh + \sinh 2kh)} \tag{4}$$

$$\omega^2 = gk\tanh kh \tag{5}$$

in which k is the wave number, defined by the dispersion relationship of progressive waves Eq. (5). The angular frequency of the wave is ω, h is the wave basin depth, l is the distance between the center of flap rotation and the tank bottom and θ is the angle of wave propagation. In the present case, h = 4.1 m and l = −2.89 m (negative values is for positions above the bottom). Different sides of the basin have a different angle of propagation considering the same basin reference. That way, θ is related to each side. The geometrical relationship between θ and k become $k_x = k\cos\theta$ and $k_y = k\sin\theta$.

The evanescent wave mode is the result of an infinite summation of terms as:

$$FT_e = \sum_{j=1}^{\infty} c_{sj} \frac{k_{sj}}{\sqrt{k_{sj}^2 + k_y^2}} \tag{6}$$

where C_{sj} is given by:

$$c_{sj} = \frac{-4\sin k_{sj}h[\cos k_{sj}(-l) - \cos k_{sj}h + k_{sj}(-2l)\sin k_{sj}(-l) - k_{sj}(h+l)\sin k_{sj}h]}{k_{sj}(h+l)(2k_{sj}h + \sin 2k_{sj}h)} \tag{7}$$

The terms k_{sj} are the solutions of the dispersion relationship of evanescent waves given by:

$$\omega^2 = -gk_s\tan k_s h \tag{8}$$

Normally, a finite number of terms are used to evaluate the transfer function with sufficient accuracy. The magnitude and phase of the theoretical transfer function is shown in Fig. 4.1 in blue lines. The experimental measurements present a delay due to the communication network (t_{Net} = 12.00 ms), wave probes signal conditioning (t_{WP} = 9.60 ms) and analog transmission (t_{Ta} = 8.30 ms). Hence, the total delay time introduced by the automation system in the present experiment may be given by the summation of those delays resulting in:

$$t_d = t_{WP} + t_{Ta} + t_{Net} = 9.60\text{ ms} + 8.30\text{ ms} + 12.00\text{ ms} = 29.90\text{ ms} \tag{9}$$

Furthermore, the motor control loop response must also be considered, represented by a second order transfer function as explained before.

Fig. 4.1 shows the frequency response plot of the wave generation transfer function, considering the waves measured on the flaps surface. Several waves described in Table 4.1 were considered in the test, with four values of steepness (H/L) and nine frequencies. A limited time window was used to exclude the reflection of waves to the other side of the basin in this analysis. Time window (t_R) was evaluated by the time necessary for the waves to travel the basin length and to come back, considering the wave group velocity. The encoder measures the flap stroke movement and the ultrasonic wave probe measures the wave elevation. The cross spectrum between these signals is the complex FT experimentally obtained. In this test, an average between all the wave probes on side 1 was used to evaluate the average FT. Fig. 4.1 shows the magnitude and phase plots and gets consistently similar to the theory when the 29.90 ms delay and the servo-motor dynamics are considered in the theoretical transfer function, indicating the consistency of the whole analysis.

4.2. Absorption algorithm

The method used to absorb reflected waves inside the basin is responsible for stabilizing the wave field in the middle of the basin for a long period of time, considering reflected waves from the model or from the opposite side of the basin.

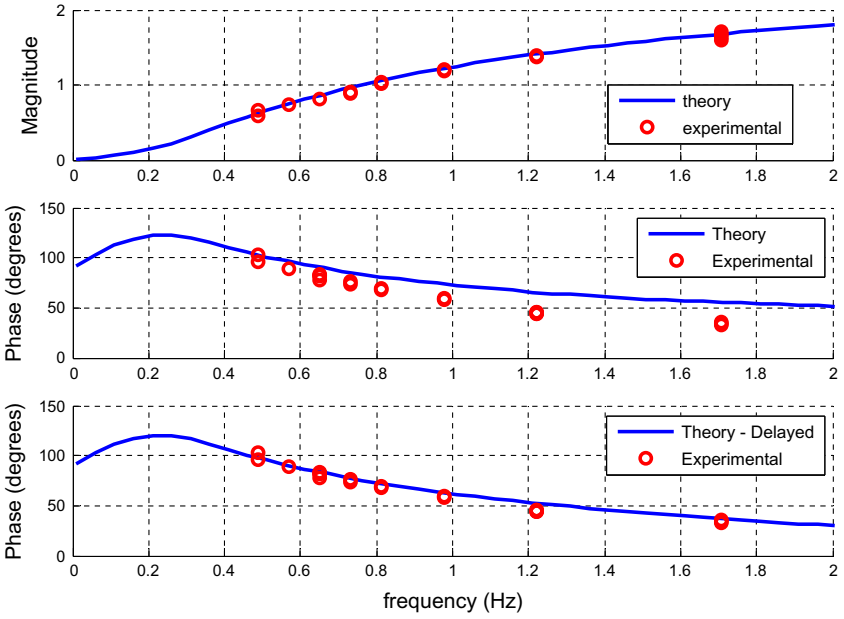

Fig. 4.1. Wave flap response transfer function – comparison between theory and experimental values: (up) magnitude of the FT; (middle) phase of the FT; (down) phase of the FT considering the delay introduced by automation.

Table 4.1
Wave characteristics in the flap wave elevation test.

Frequency (Hz)	Steepness H/L (%)	L (m)	t_R (S)
1.67	2–3–4–6	0.56	60
1.25	2–3–4–6	1.00	45
1.00	2–3–4–6	1.56	36
0.83	3–6	2.25	30
0.71	3–6	3.06	26
0.63	2–3–4–6	4.00	23
0.56	2–3	5.06	20
0.50	2	6.25	18
0.45	2	7.54	16

The work by Maeda et al. [7], Zhang [18] and [19] describe a method to separate the effects of wave generation and absorption in order to generate and absorb waves simultaneously. This is normally called "dual mode". The flap movement creates an elevation of wave in front of the flap. If is possible to synthesize the time series of the flap movement, it is also possible to synthesize the time series of the wave elevation in front of the flap (using the FT previously discussed, taking into account the response of the automation system). This statement is valid for linear waves and can also be extended to the non-linear wave theory. Therefore, it is possible to generate non-linear waves simultaneously with linear wave absorption methods.

In the present work, the linear wave generation theory was adopted including the hypotheses of superposition of harmonic waves to create spectral sea states. To absorb waves, the linear theory was also adopted to create a digital filter, as described latter. The "dual mode" was applied since this approach allows the application of different theories for wave generation (including second order wave theory).

Fig. 4.2 shows irregular wave elevation synthesized (nd) compared to the wave probe measurement (nk). The irregular wave was recorded by the central wave probe on side 1 of the basin for a perpendicular wave. The flap movement time series was

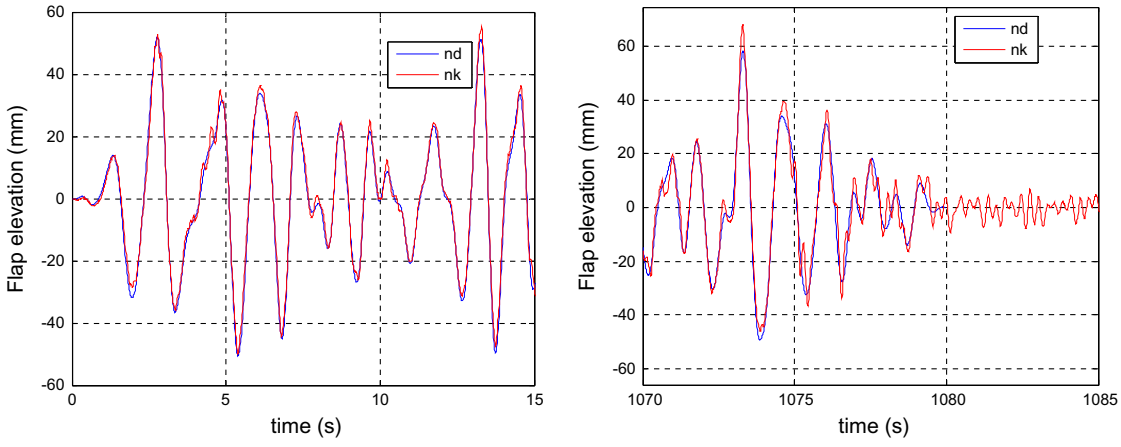

Fig. 4.2. Irregular wave elevation close to the flaps (Tp = 1.56 s, H_s = 78.4 mm and γ = 1.664).

synthesized according to [13], that derives the method of summation of the spectral components with random phase shifts. The recommendations of Miles and Funke [9] and Chakrabarti [3] for synthesizing sea wave time series were considered. The energy density spectrum was defined from a typical storm sea state of the Campos Basin in Brazil in a 1:100 scale.

As already mentioned, the time series of wave elevation (nd) was obtained from the flap movement and the FT transfer function, including the dynamic response of the automation system. It is possible to verify that the measured (nk) and expected (nd) wave elevation series are very close for both time windows, indicating that the derived transfer function FT in Section 4.1 is quite accurate.

In the first seconds of the test (Fig. 4.2a), there are no reflected waves on the opposite side of the tank, and the adherence between the series are even better. For the second time window (Fig. 4.2b), the waves already reached the opposite side of the tank and came back. Since the absorption algorithm (that will be explained latter) is properly working, very small differences between the theoretic and measured wave elevation can be seen.

The "dual mode" method uses the estimated wave elevation (nd) and the wave elevation (nk) to estimate the reflected wave as nr = nk–nd for each flap. The reflected wave (nr) is the input to the absorption filter. The ideal absorption filter works as an inverse of function FT in a closed loop between wave elevation in front of the flap and flap movement [17]. The wave elevation causes the flap movement and prevents the wave from reflecting back as a transparent frontier for waves, as an infinite basin without borders. The frequency domain block diagram of the absorption is presented in Fig. 4.3, in which the time domain signals are also indicated.

F is a complex transfer function related to the inverse of the flap generation transfer function given by:

$$F = \frac{-i}{FT_p + iFT_e} \tag{10}$$

This exact filter is impossible to be synthesized since the process is non-causal [4]. So, a digital filter was optimized and the implementation of the absorption filter in time domain is made by a non-recursive FIR digital filter:

$$\widetilde{F} = \sum_{l=-M_2}^{M_2} \sum_{k=0}^{M_1} a_{k,l} z_1^{-k} z_2^{-l} \qquad z_1 = e^{i\omega\Delta t}; \quad z_2 = e^{i\omega\Delta y} \tag{12}$$

where Δy is the distance between two adjacent wave probes. The coefficients $a_{k,l}$ can be obtained by an optimization algorithm that matches $\widetilde{F}$ and F. The optimization procedure considered wave directions from $\theta = 0^o$ to 75^o (with steps of 15^o), in a frequency range from 0 to 2.0 Hz for $\theta = 0^o$. Biesel limit [1] was considered for defining the frequency range for all the others wave directions. The absorption of oblique waves ($\theta \neq 0^o$) is achieved through the utilization of the adjacent flaps wave probes. In this study, $M_2 = 2$, then each flap actuation uses its own wave probe and the two adjacent wave probes on each side. The actuation also depends on the actual and the 300 previous measurements ($M_1 = 300$).

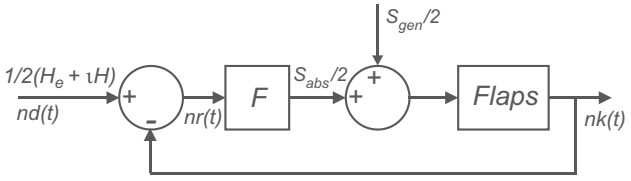

Fig. 4.3. Absorption system block diagram.

Another advantage of the "dual mode" method can be identified at this point. The "single mode" uses the same function $\widetilde{F}$ both for wave generation and absorption. This can introduce errors in the generated wave, since the exact absorption function F cannot be synthesized, and $\widetilde{F}$ is an approximation for the exact function. In the "dual mode", the exact expressions can be used for wave generation (expressions (2)–(4)) and the approximation error of $\widetilde{F}$ and F will only affect the absorption performance.

The quality of absorption is quantified by the reflection coefficient (Cr). The value of Cr is estimated in experimental tests by an auto-check described by Schäffer [15], from the responses of the motor encoder and the wave elevation (nk). The auto-check compares the ideal response with the real response and the difference is the coefficient of reflection. More details about the absorption algorithm can be found in Carneiro et al. [2].

Fig. 4.4 shows the theoretical reflection coefficient (lines) and experimental values for regular waves (dots). Three frequencies (0.7, 1.0 and 1.3 Hz) and four angles of absorption (colors) were considered. It is expected that above the Biesel Limit, described in Biesel [1], it is impossible to generate and to absorb waves, related to the finite width of the flaps. For the present case, this limit is 1.43 Hz for 45^o wave propagation. The reflection coefficient is very large for frequencies higher than this limit. Thus, the optimized filter can provide less than 10% of reflection for frequencies up to 1.43 Hz and directions between 0^o and 45^o.

A qualitative evaluation of the absorption algorithm is shown in Fig. 4.5. A time lapse comparing a regular wave, with and without absorption, in the basin is presented. It is possible to note the wave elevation that creates a standing wave pattern without absorption. This standing wave did not dissipate because the frontiers of the basin reflect back almost all the wave energy. With absorption active, almost all the wave energy was absorbed.

4.3. Irregular long-crested sea states

Several irregular long-crested sea states were reproduced in the tank to validate the generation/absorption of waves. Two examples of long-crested sea states are shown in Fig. 4.6. The figures present the desired energy spectrum and the experimental spectrum, which is obtained by a capacitive wave probe located in the middle of the basin. These waves represent typical centenary conditions of the Campos Basin and the Santos Basins in Brazil. The first wave was reproduced at scale 1:100 and the second wave at scale 1:120, with a 3-h duration in real scale. Very good adherence

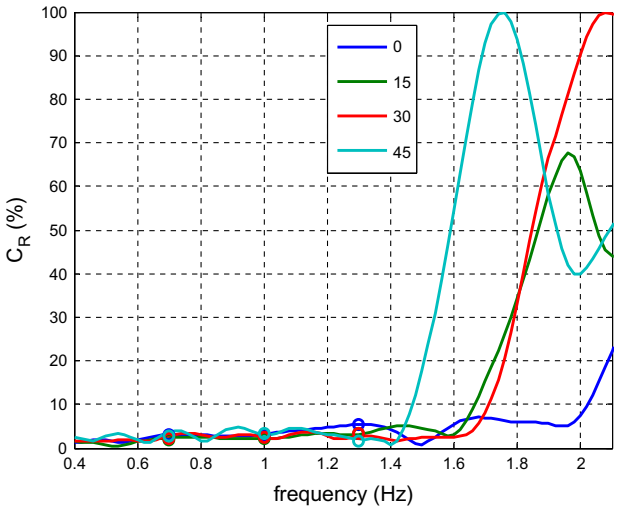

Fig. 4.4. Reflection coefficient – experimental and theoretical values.

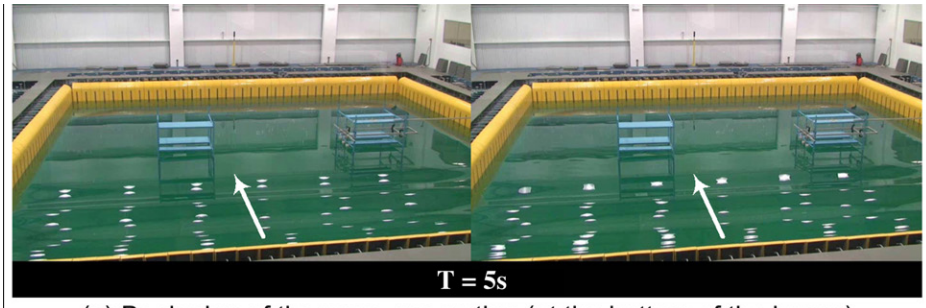

(a) Beginning of the wave generation (at the bottom of the image).

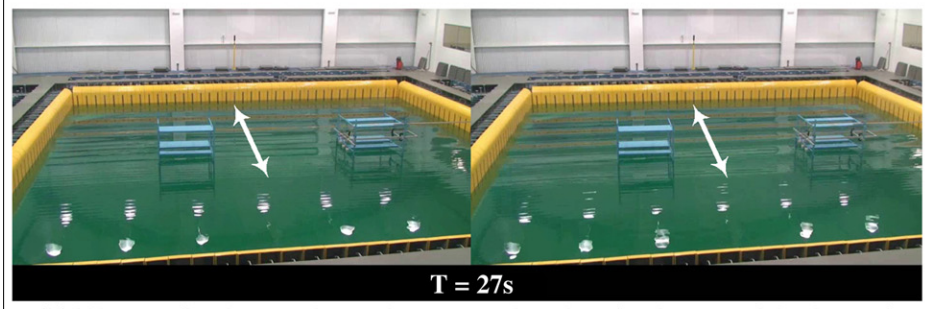

(b) Wave reflection on the active wave absorber (at the top of the image).

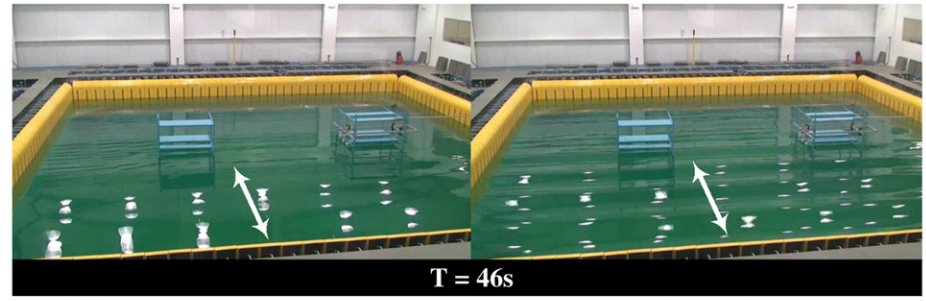

(c) Wave reflection on the wave generator (at the bottom of the image).

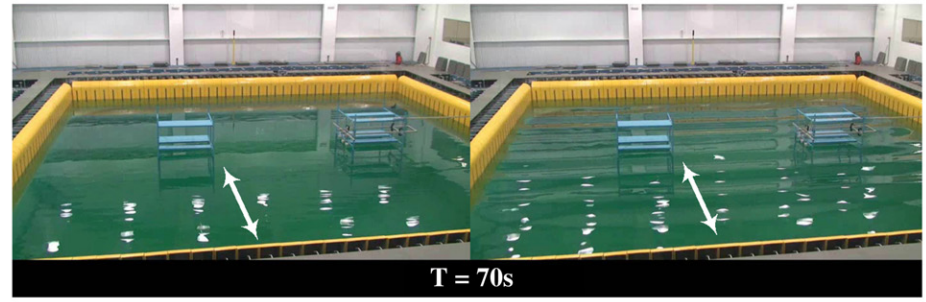

(d) Second wave reflection on the wave generator (at the bottom of the image).

Fig. 4.5. Comparison between the tank with (left side) or without (right side) active wave absorption. In the case of active absorption, only the upper side absorbs wave. The underside generates 1 Hz waves for 18 s and then stops.

between desired and experimental curves is verified for both cases. The wave peak period (T_p) and the significant wave height (H_S), parameters normally verified to define an irregular wave, are also quite similar to the desired values. The differences are smaller than 2.4% for H_S and 0.5% for T_p.

4.4. Oblique regular waves

In order to verify the quality of waves in angles, several tests with regular waves were conducted. Different regular waves of 0.7 Hz, 1.0 Hz and 1.3 Hz were generated in angle between sides 1 and 4 ($\theta = 0^o$, 30^o, 45^o). Three different wave steepnesses were considered (2.5%, 3.3% and 5.0%), resulting in a total of 27 waves tested (see Table 4.2).

In order to verify the wave propagation direction, an array of capacitive wave probes was used, with the method described in Nwogu [14]. It uses the cross spectra between wave probes in an array configuration to evaluate the energy directional spreading and the mean direction, using the Maximum Entropy Method (MEM).

The signal time window excluded the reflection of waves on the opposite side of the basin. Thus, four cycles could be used for the 0.7 Hz waves, eight cycles for 1.0 Hz and 14 cycles for 1.3 Hz. For regular waves, these numbers of cycles are acceptable for estimating the direction. Furthermore, in the original work by Nwogu [16],

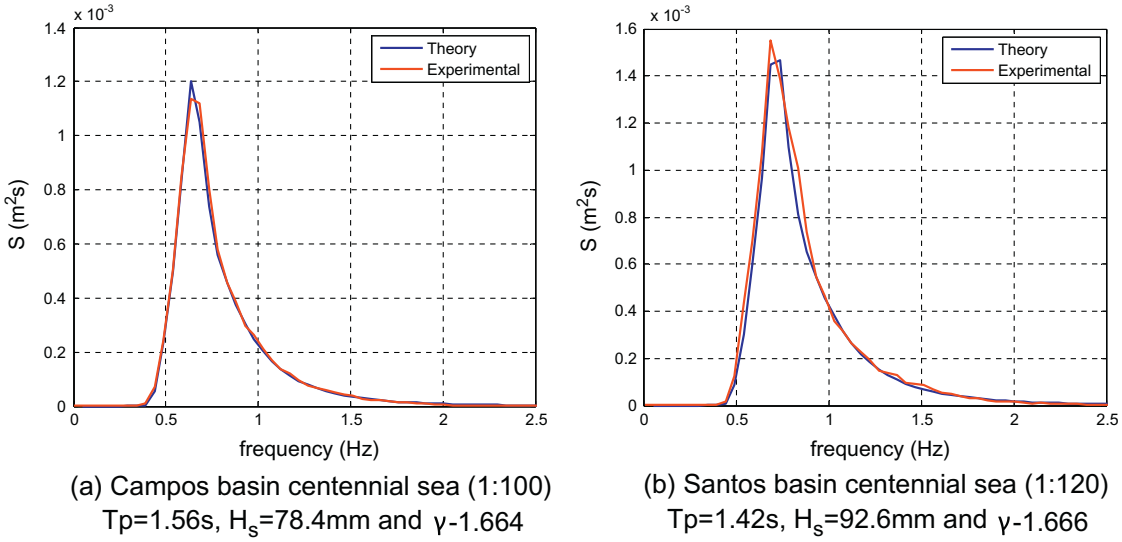

Fig. 4.6. Density of energy spectrums of irregular long-crested waves.

Table 4.2
Characteristics of waves in the regular oblique wave experiment.

Name	Frequency (Hz)	Steepness H/L (%)/Height (mm)	Directions (degree)
Wave01	0.7	2.5%/79.6 mm	0–30–45
Wave02		3.3%/106.2 mm	
Wave03		5.0%/159.3 mm	
Wave04	1.0	2.5%/39.0 mm	
Wave05		3.3%/52.0 mm	
Wave06		5.0%/78.1 mm	
Wave07	1.3	2.5%/23.1 mm	
Wave08		3.3%/30.8 mm	
Wave09		5.0%/46.2 mm	

a 5-wave probes array was used, being one in the central position and the others distributed around it. In that case, four cross spectrum functions were considered by the MEM, with the central sensor signal combined with each of the other sensors. In the present case, the utilization of a 9-wave probe array results in a more accurate result, since eight cross spectrum functions are considered in the MEM. Also, in order to improve the quality of the cross spectra considering the limited number of wave cycles, a sampling rate of 50 Hz was adopted with 10 times over-sampling.

Fig. 4.7 shows the array of wave probes, and the distance between each probe is 1 m. The wave propagation (θ) direction is defined in Fig. 4.7. The experimental wave propagation direction was close to the desired direction, as shown in Fig. 4.8. The maximum difference is 2°, which can be considered quite acceptable.

The average measurement of the wave probes around the center of the basin (wave probes 4, 5, 7 and 8 in Fig. 4.7) was used to estimate the height of each wave. Fig. 4.9 shows the experimental waves height for all the waves tested. The wave height presents less than 5% deviation, as compared to the desired value.

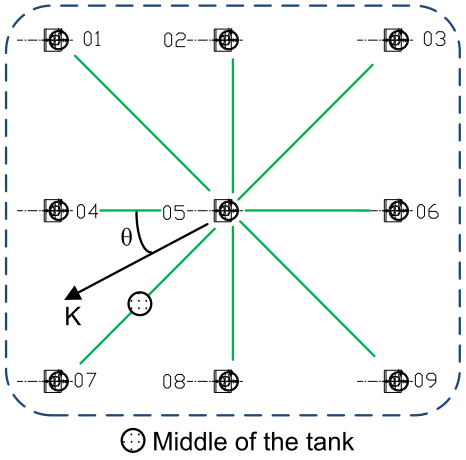

Fig. 4.7. Array of wave probes close to the middle of the basin.

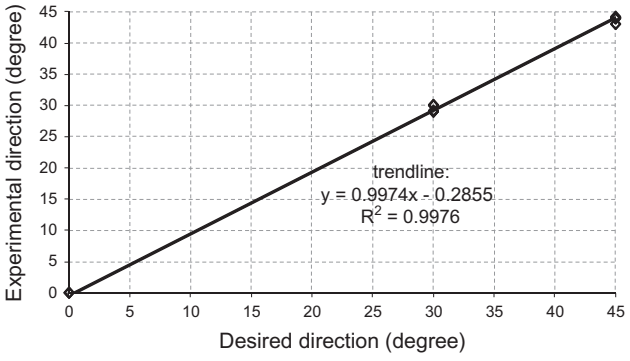

Fig. 4.8. Wave propagation directions in the middle of the basin.

4.5. Multidirectional wave generation

Fig. 5.0 shows two examples of experimental wave generation to demonstrate the accuracy and the precision of the automation system, considering complex cases of multidirectional waves. A concentric wave focusing on a location inside the wave basin is an illustrative example of the system accuracy and synchronization, shown in Fig. 5.0a and b shows an interference of waves with the pattern of the Brazilian Flag on the water surface.

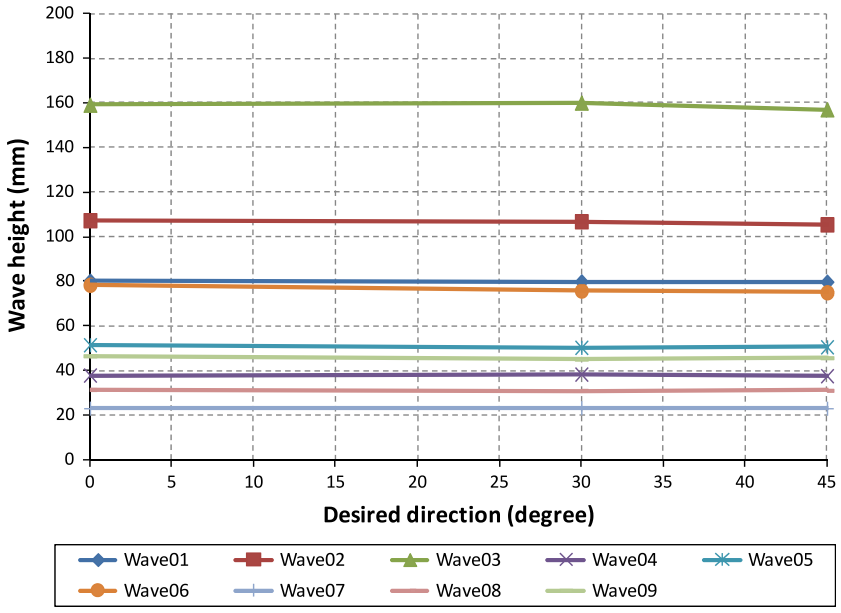

Fig. 4.9. Wave height measure in the middle of the basin.

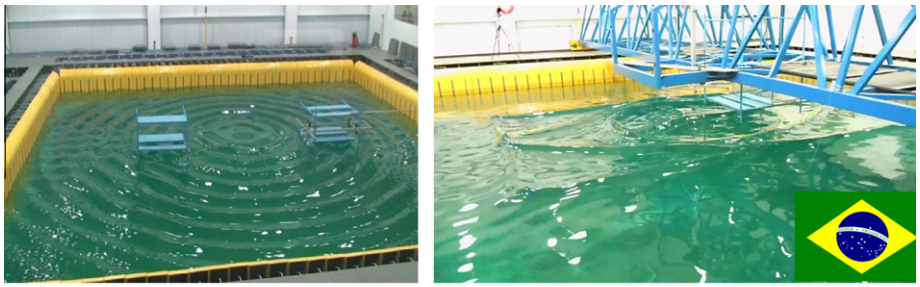

Fig. 5.0. Examples of multidirectional waves in wave basin.

5. Conclusions

The control and automation system presented herein was applied in a wave tank with 148 active hinged flaps, and was shown to work properly. The predicted performance of the hardware was compared to the experimental observation considering the final set-up, and a good adherence between the time-delays was verified. The 12.00 m scan time and the total 29.90 m delay are adequate for performing the generation and absorption control algorithms, as demonstrated in the results presented.

The utilization of industrial automation equipment is a promising solution for wave tanks, due to properties of robustness, reliability, ease of maintenance and replacement of parts. Furthermore, expansion to a larger number or actuators or sensors may also be carried out easily, keeping the architecture and the solution developed for future works.

Acknowledgements

The authors acknowledge Petrobras for the financial support and for the motivation of this work. The authors also acknowledge the Brazilian research funding agencies: São Paulo State Research Foundation (FAPESP), National Council for Scientific and Technological Development (CNPq) and Research and Projects Financing (FINEP) for the research grants and for the constant support.

References

[1] Biesel F. Wave machines. In: Proceedings 1st conference on ships and waves. Hoboken (NJ); 1954.
[2] Carneiro ML, de Mello PC, Tannuri EA. USP active absorption basin: absorption of irregular waves. In: Proceedings of the ASME 30th international conference on ocean, offshore and arctic engineering – OMAE. Rotterdam (The Netherlands); 2011.
[3] Chakrabarti SK. Hydrodynamics of offshore structures. Southampton (UK): WIT Press; 1987.
[4] Chatry G, Clément AH, Gouraud T. Self-adaptative control of a piston wave absorber. In: Proceedings of eighth international offshore and polar engineering conference – ISOPE; 1998. p. 127–33.
[5] de Mello PC. Um aparato para redução da reflexão de ondas em praia Parabólica. M.Sc. Dissertation (in Portuguese); 2006. p. 117. [COPPE, Federal University of Rio de Janeiro].
[6] Dean RG, Dalrymple RA. Water wave mechanics for engineers and scientists. Englewood Cliffs (New Jersey): Prentice-Hall, Inc.; 1984.
[7] Maeda K, Hosotani N, Tamura K, Ando H. Wave making properties of circular basin. In: International symposium on underwater technology; 2004.
[8] Martins JA de A, de Mello PC, Carneiro ML, Souza CAGF, Adamowski JC. Laboratory wave probes dynamic performance evaluation. In: Proceedings of XX COPINAVAL – Congresso PanAmericano de Engenharia Naval e Transportes Marítimos; 2007.
[9] Miles MD, Funke ERA. Comparison of methods for synthesis of directional seas. J Offshore Mech Arctic Eng 1989;111(43).

[10] Mitsubishi. General-Purpose AC Servo Melservo J3 series – Instruction Manual. SH-NA-030051-C (Mitsubishi Electric Corporation), 2007.
[11] Naito S. Wave generation and absorption in wave basins: theory and application. In: Proceedings 16th international offshore and polar engineering conference. San Francisco (California, USA); 2006.
[12] Naito S, Nakamura T, Sakashita H, Tomita K. A new configuration of wave basin and a control of wave generation and absorption – the case when an advancing ship comes across the given waves. In: Proceedings of the 4th Pacific/Asia offshore mechanics, symposium; 1996.
[13] Nohara BT, Yamamoto I, Matsuura M. The organized motion control of multi-directional wave maker. In: Proceedings of the 4th international workshop on advanced motion, control; 1996.
[14] Nwogu O. Maximum entropy estimation of directional wave spectra from an array of wave probes. Appl Ocean Res 1989;11(4):1989.
[15] Schäffer HA. Active Wave Absorption in Flumes and 3D Basins. In: Proceedings of 4th int. symp. on ocean wave measurement and analysis. San Francisco (USA); 2001.
[16] Schäffer H, Klopman G. Review of multidirectional active wave absorption methods. J Waterway, Port, Coastal, Ocean Eng, ASCE 2000.
[17] Schäffer H, Skourup J. Active absorption of multidirectional waves. In: Proc., 25th int. conf. on coast. engrg., ASCE; 1996.
[18] Zhang H. A deterministic combination of numerical and physical models for coastal waves. Tese (Doctor of Philosophy), Lyngby (Denmark): Technical University of Denmark, Maritime and Structural Engineering; 2005. p. 145.
[19] Zhang H, Schäffer HA, Jakobsen KP. Deterministic combination of numerical and physical coastal wave models. J Coastal, Harbour Offshore Eng 2007.